Inorganic Chemistry

pubs.acs.org/IC

Article

Synthesis, Characterization, and Reactivity of Bispidine-Iron(IV)-Tosylimido Species

Thomas Josephy,[#] Ravi Kumar,[#] Katharina Bleher, Fridolin Röhs, Thorsten Glaser, Gopalan Rajaraman,* and Peter Comba*

Cite This: *Inorg. Chem.* 2024, 63, 12109−12119

Read Online

ACCESS | Metrics & More | Article Recommendations | Supporting Information

ABSTRACT: Reported are the synthesis and detailed studies of the iron(IV)-tosylimido complexes of two isomeric pentadentate bispidine ligands (bispidines are 3,7-diazabicyclo[3.3.1]nonane derivatives). This completes a series of five tosylimido complexes with comparable pentadentate amine/pyridine ligands, where the corresponding $[(L)\text{-}Fe^{IV}{=}O]^{2+}$ oxidants have been studied in detail. The characterization of the two new complexes in solution (UV−vis-NIR, Mössbauer, HR-ESI-MS) shows that these oxidants have an intermediate spin (S = 1) electronic ground state. The reactivities have been studied as oxidants in C−H activation at 1,3-cyclohexadiene and nitrogen atom transfer to thioanisole. For the latter substrate, the entire set of data for the five ligands and for both nitrogen and oxygen atom transfer is now available and the interesting observation is that oxygen atom transfer is, as expected, generally faster than nitrogen atom transfer, with the exception of the two ligands that have four and three pyridine groups oriented parallel to the Fe−O and Fe−N axes. A thorough DFT analysis indicates that this is due to steric effects in the case of the $[(L)Fe^{IV}{=}O]^{2+}$ species, which are less important in the $[(L)Fe^{IV}{=}NTs]^{2+}$ compounds due to partial electron transfer from the thioanisole substrate to the iron(IV)-tosylimido oxidant.

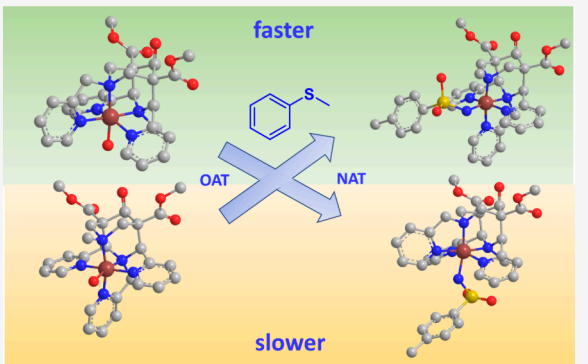

INTRODUCTION

High-valent heme and nonheme metal−oxygen and metal−nitrogen species are highly efficient oxidants in enzymes;[1−3] they are active oxidants in environmentally important abiotic natural processes[4−6] and are used in industrially relevant catalytic oxidations.[7,8] Nonheme iron-oxido complexes have been known for two decades[9−11] with a large data and knowledge base, involving iron in various oxidation and spin states[2,3,12,13] and also involving superoxido and peroxido species.[14−16] This includes mono- as well as dinuclear complexes with various reactivity patterns related to structural and electronic properties, probed by kinetic, electrochemical, and spectroscopic experiments as well as quantum-chemical calculations.[3,17,18] Trapping and characterization of the corresponding metal−nitrogen species only started a decade ago, and thorough structural, spectroscopic, and reactivity data is still relatively scarce.[19,20] High-valent metal-nitrene, -nitride, -amido, or -imido complexes are of potential use for nitrene transfer and C−N formation reactions and therefore of interest for the aziridination and amination of alkenes and alkanes, processes for which complexes of copper, manganese, and specifically also of iron have been shown to be of interest.[21−29]

There are only a few structurally characterized iron-nitrene or imido species,[30−33] but a number of spectroscopically characterized compounds have been published.[29,32,34] Moreover, the reactivity of a range of iron−nitrogen oxidants was compared with the analogous iron−oxygen species. The iron(IV)-tosylimido complexes have, in general, been found to be more sluggish oxidants than the corresponding iron(IV)-oxido complexes, particularly in C−H abstraction reactions,[35] but sulfoxidations, for instance, can be significantly faster for the iron(IV)-tosylimido complexes than the corresponding oxido species,[36] and this has been related to large differences in the electron transfer properties.[36,37]

Among the most thoroughly studied nonheme systems with pentadentate amine/pyridine ligands in iron(IV)-oxido oxidation and oxygenation chemistry are N_4py (named L^1 in the text), BnTPEN (L^2), the two isomers Me_2CHpy_2TACN (L^3) and $Mepy_2TACN$ (L^4), and the two isomeric bispidines $N_2py_3{}^u$ (L^5) and $N_2py_3{}^o$ (L^6) (see Scheme 1).[38] The iron(IV)-oxido species with a tetradentate bispidine derivative and a chlorido or bromido coligand are the most reactive ferryl complexes, with hydrogen abstraction rates (HAA) for the

Received: March 27, 2024
Revised: May 23, 2024
Accepted: June 7, 2024
Published: June 14, 2024

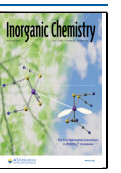

https://doi.org/10.1021/acs.inorgchem.4c01237
Inorg. Chem. 2024, 63, 12109−12119

Scheme 1. Ligands Discussed in This Work (the Numbering Scheme in Bispidines is Given in L^6)[a]

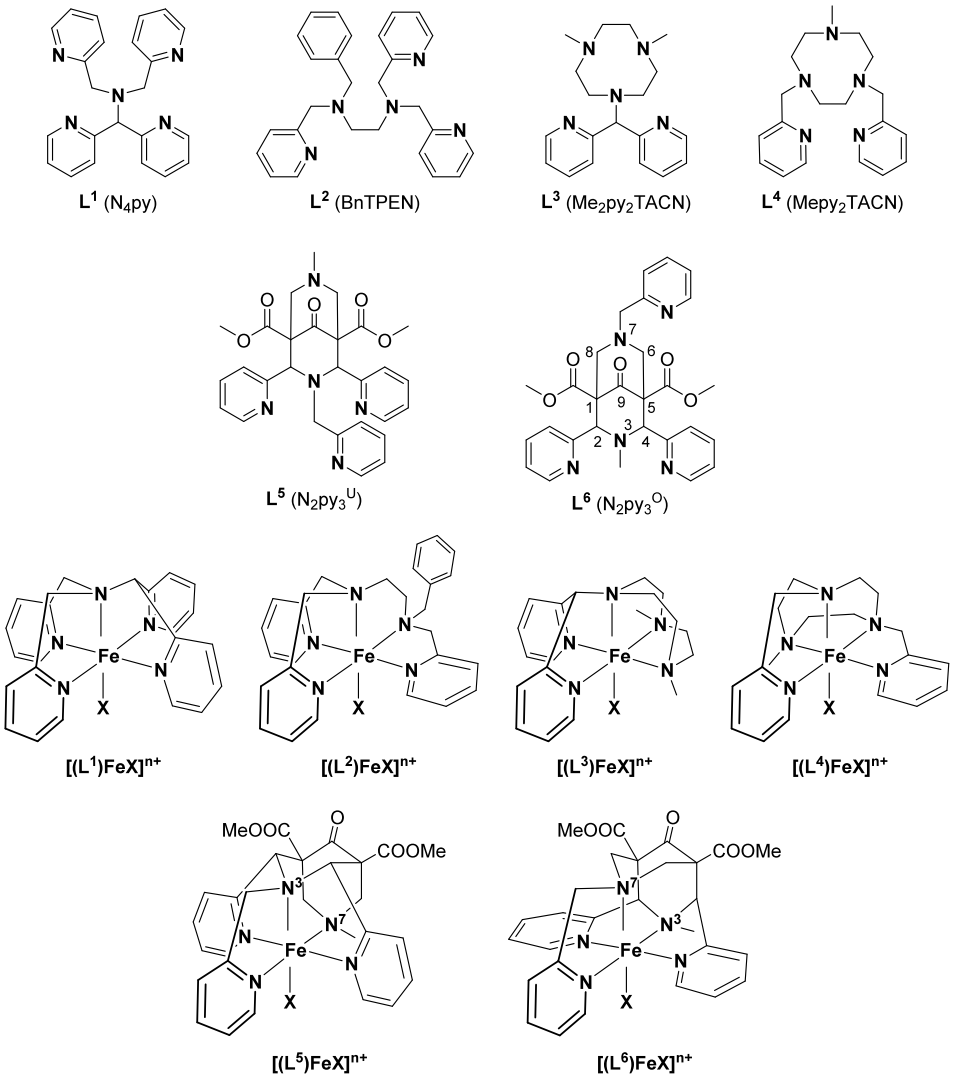

[a]Also shown are sketches of the geometries of the corresponding iron complexes, all with a vertical *z*-axis (iron(II) precursors, where X is a solvent molecule, *e.g.*, $[(L^1)Fe^{II}(NCMe)]^{2+}$, iron(IV)-oxido, where X is the oxido group, *e.g.*, $[(L^1)Fe^{IV}{=}O]^{2+}$, iron(IV)-tosylimido, where X is a tosylimido group, *e.g.*, $[(L^1)Fe^{IV}{=}NTs]^{2+}$.

difficult to oxidize substrate cyclohexane (BDE = 99.5 kcal/mol, selective halogenation)[39] that are comparable to those of enzymes ($t_{1/2}$ = 3.5 s, EtCN, −90 °C).[40−42] One possible reason for this exceptional reactivity is the very rigid bispidine scaffold with a cavity too large for the $Fe^{IV}{=}O$ center, leading to a high $Fe^{IV/III}$ redox potential and, hence, a large driving force. In addition and importantly, there is a very small triplet−quintet gap in $[(L)Fe^{IV}{=}O(Cl)]^+$ with the tetradentate bispidine, which significantly enhances the rate of spin crossover to the quintet surface, a process that is responsible for the rate-determining hydrogen atom abstraction, and this emerges from a detailed ligand field analysis.[40−42] Among the five pentadentate ligand systems $[(L^1)Fe^{IV}{=}O]^{2+}$, $[(L^2)Fe^{IV}{=}O]^{2+}$, $[(L^3)Fe^{IV}{=}O]^{2+}$, $[(L^5)Fe^{IV}{=}O]^{2+}$, and $[(L^6)Fe^{IV}{=}O]^{2+}$, the latter with the bispidine L^6 is the fastest, and this has again been related to the driving force.[38] These five systems have also been analyzed in a detailed quantum-chemical study, involving density functional theory (DFT) and *ab initio* calculations, to better understand the fundamental reasons for the observed structure−reactivity correlation of these systems and possible implications for the ligand design for ferryl oxidants with specific reactivities.[43] Importantly, the most thoroughly studied iron(IV)-tosylimido complexes include three of the above systems, i.e., $[(L^1)Fe^{IV}{=}NTs]^{2+}$,[29,32,34−37] $[(L^2)Fe^{IV}{=}NTs]^{2+}$,[35] and $[(L^3)Fe^{IV}{=}NTs]^{2+}$ (together with $[(L^4)Fe^{IV}{=}NTs]^{2+}$).[29,32,34] Therefore, we now present experiments involving the preparation, characterization, and analysis of the reactivity of the corresponding bispidine systems $[(L^5)Fe^{IV}{=}NTs]^{2+}$ and $[(L^6)Fe^{IV}{=}NTs]^{2+}$, combined with a computational analysis of the series $[(L^1)Fe^{IV}{=}NTs]^{2+}$, $[(L^2)Fe^{IV}{=}NTs]^{2+}$, $[(L^3)Fe^{IV}{=}NTs]^{2+}$, $[(L^5)Fe^{IV}{=}NTs]^{2+}$, and $[(L^6)Fe^{IV}{=}NTs]^{2+}$.

EXPERIMENTAL SECTION

Materials and Methods. All chemicals and reagents were purchased from commercial sources (ABCR, ACROS, Sigma-Aldrich, and TCI). Dry acetonitrile was purified using an MB SPS 5 solvent purification system from MBRAUN. Air-sensitive materials were prepared and handled using either Schlenk techniques or in a glovebox under an Ar atmosphere. The oxidant *N*-(*p*-toluenesulfonyl)imino-phenyliodinane (PhINTs) was synthesized

https://doi.org/10.1021/acs.inorgchem.4c01237
Inorg. Chem. 2024, 63, 12109−12119

according to the procedures of Yamada et al. and Evans et al., washed with dichloromethane, and stored in a glovebox at −30 °C under argon until its use.[44−46]

HR-ESI-MS experiments were carried out on an ApexQe hybrid 9.4 T FT-ICR instrument from Bruker. Tandem mass experiments were carried out on a timsTOF fleX mass spectrometer from Bruker. For MS and tandem MS measurements, samples with an iron complex concentration of 10^{-5} M were prepared. For the investigation of the oxidized iron species, the reactions were carried out under the same conditions as used for the other measurements (in dry MeCN in a glovebox under argon) and were diluted accordingly for the MS measurements (for details, see Supporting Information). The measurements were carried out by the Mass Spectrometry Facility, Department of Chemistry, University of Heidelberg, Heidelberg, Germany.

Elemental analyses were performed on a CHN-O vario EL by the "Mikroanalytisches Labor", Department of Chemistry, Heidelberg University, Heidelberg, Germany.

UV−vis−NIR spectra were recorded on an Agilent 8453 spectrophotometer equipped with a *USP-203-A* cryostat from Unisoku.

^{57}Fe Mössbauer spectra were recorded on an alternating constant-acceleration spectrometer using iron-57-enriched samples. The minimal line width was 0.24 mm s^{-1} full-width at half-height. The sample temperature was maintained constant in a bath cryostat (Wissel MBBC-HE0106). ^{57}Co/Rh was used as the radiation source. Isomer shifts were determined to be relative to α-iron at room temperature.

In general, spectra were processed with OriginPro 2020.

Preparation of the Ligands and Complexes. The ligands and iron(II) complexes used were synthesized according to literature-known procedures of Comba et al. and characterization by NMR, ESI-MS, and EA.[47−49]

[Fe^{II}L^5](OTf)$_2$. EA ($C_{32}H_{32}FeF_6N_6O_{11}S_2 \times 2H_2O$) [%]: calc.: C, 40.60; H, 3.83; N, 8.88; found: C, 40.80; H, 3.89; N, 8.59. HR-ESI-MS (pos., MeCN): m/z = 720.1030 (100%) (calcd: 720.1033) [Fe^{II}L^5 + OTf]$^+$.

[Fe^{II}L^6 MeCN](OTf)$_2$. EA ($C_{32}H_{32}FeF_6N_6O_{11}S_2 \times 2H_2O$) [%]: calc.: C, 40.60; H, 3.83; N, 8.88; found: C, 40.65; H, 3.74; N, 8.31. HR-ESI-MS (pos., MeCN): m/z = 606.1190 (99%) (calc: 606.1201) [Fe^{II}L^6 + Cl]$^+$, m/z = 624.1295 (100%) (calc: 624.1307) [Fe^{II}L^6 + Cl + H_2O]$^+$.

[^{57}Fe^{II}L^5 MeCN](OTf)$_2$. EA ($C_{32}H_{32}FeF_6N_6O_{11}S_2 \times$ MeOH $\times$ 0.5H_2O) [%]: calc.: C, 41.60; H, 3.91; N, 8.82; found: C, 41.67; H, 3.97; N, 8.74. HR-ESI-MS (pos., MeCN): m/z = 721.1038 (100%) (calcd: 721.1037) [Fe^{II}L^5 + OTf]$^+$.

[^{57}Fe^{II}L^{6}H$_2$O](OTf)$_2$. EA ($C_{30}H_{31}{}^{57}FeF_6N_5O_{12}S_2 \times$ 0.25MeCN $\times$ 0.5H_2O) [%]: calc.: C, 40.35; H, 3.64; N, 8.10; found: C, 40.38; H, 3.72; N, 8.06. HR-ESI-MS (pos., MeCN): m/z = 607.1207 (100%) (calcd: 607.1206) [Fe^{II}L^6 + Cl]$^+$.

Kinetics. Kinetics were measured using an iron complex concentration of 0.5 mM, which were treated with the required amount of the oxidant. Once the maximum concentration of the oxidized species was reached, the substrate was added and the reaction was monitored based on the respective characteristic absorption band of the iron tosylimido species using UV−vis−NIR spectroscopy. Each measurement was performed at least three times. Subsequently, the second-order reaction rate constant (k_2) was determined from the average values of the rate constants (k_{obs}) versus the substrate concentration (for details, see the SI).

Computational Work. All the calculations are performed using established procedures[29,35,50−53] with Gaussian 09 (Revision A.02)[54] and ORCA 4.2.1 programs.[55,56] For geometry optimization, Grimme's dispersion corrected unrestricted B3LYP functional (UB3LYP-D2)[57] using a double ζ-quality LanL2DZ basis set with Los Almos effective core potential for Fe, and 6-31G* for N, H, C, O, and S.[58−61] Single-point energy calculations are performed with TZVP for all of the atoms. Solvation effects are computed using the polarizable continuum model (PCM) employing acetonitrile as the solvent.[62] Solvent phase optimization for [(L^6)Fe^{IV}=NTs]$^{2+}$ has been performed to ascertain the role of solvent during optimization, and this yields a quintet−triplet gap of 21.2 kJ/mol, suggesting only minor alterations (see Supporting Information, Table S9). In short, we have employed the UB3LYP-D2/TZVP(PCM)//UB3LYP-D2/LanL2DZ-(Fe),6-31G*(rest atoms) level of theory.

The Mössbauer isomer shift (δ) and quadrupole splitting ($|\Delta E_Q|$) were calculated at the UB3LYP(D3BJ)/CP(PPP)(Fe),def2-TZVP-(rest atoms)(CPCM(acetonitrile)) level of theory using ORCA, and δ was derived based on the calibration constants reported by Römelt et al.[29,55,63]

Coupled cluster calculations are the "gold standard", specifically for the ground-state spin of iron(IV)-oxido/nitrido complexes, but the computational costs are extremely high. The recently introduced DLPNO-CCSD(T) method provides a particularly interesting approach to circumvent this problem. The protocol used here involves the optimization of the structures with DFT, followed by single-point gas phase calculations using DLPNO-CCSD(T) to determine a corrected energy of the electronic ground and excited states for iron(IV)-tosylimido complexes [(L^n)Fe=NTs]$^{2+}$ (n = 1−3, 5, 6) and their reactant complex (RC), transition states (TS), intermediates (Int), and product complex (PC).[55,64,65]

RESULTS AND DISCUSSION

Preparation and Characterization of the Bispidine-Iron(IV)-Tosylimido Complexes. Bispidine-iron(IV)-oxido complexes in general are very reactive,[38,41,42,66,67] and their characterization usually involves solution spectroscopy, often under cryo-stopped-flow conditions or from freeze-quenched samples. In analogy, the bispidine-iron(IV)-tosylimido complexes described here were prepared in solution and characterized by time-resolved ultraviolet−visible-near-infrared (UV−vis-NIR) spectroscopy, high-resolution electrospray mass spectrometry (HR-ESI-MS), and Mössbauer spectroscopy, combined with monitoring the decay kinetics and product analyses of the metastable tosylimido complexes in the presence of organic substrates. The procedures for the preparation of solutions of the [(L^n)Fe^{IV}=NTs]$^{2+}$ complexes (n = 5, 6) following those published for similar systems:[29,34−37] the iron(II) precursors were reacted with 3 eq of *N*-(*p*-toluenesulfonyl)imino-phenyliodinane (PhINTs; dry acetonitrile (MeCN), Ar, RT; see Experimental Section and Supporting Information for details). The reactions were monitored by UV−vis-NIR spectroscopy, showing the disappearance of a charge transfer transition of the iron(II) precursor (350−450 nm) with the simultaneous formation of a new species with dd transitions in the region of 730 nm. A charge transfer band in the region of 460 nm, expected from known iron(IV)-tosylimido complexes, was only observed for [(L^6)Fe^{IV}=NTs]$^{2+}$, while [(L^5)Fe^{IV}=NTs]$^{2+}$ only shows the dd absorption, known from the bispidine-iron(IV)-oxido analogues and known iron(IV)-tosylimido species (see Supporting Information, Figures S1 and S2 for time-dependent spectra of [(L^5)Fe^{IV}=NTs]$^{2+}$ and [(L^6)Fe^{IV}=NTs]$^{2+}$, respectively). The [(L^n)Fe^{IV}=NTs]$^{2+}$ complexes (n = 5, 6) decay with time (L^6: $t_{1/2} \approx$ 8 min; L^5: $t_{1/2} \geq$ 4 h; see Supporting Information, Figures S1−S3), and solutions with maximum [(L^n)Fe^{IV}=NTs]$^{2+}$ concentrations were frozen for Mössbauer spectroscopy to support their characterization as tosylimido complexes and determine the oxidation and spin states (see Figure 1). HR-ESI-MS of samples with maximum concentration of the tosylimido species were used to determine the stoichiometry. The spectroscopic properties of the L^5- and L^6-based iron(IV)-tosylimido and -oxido complexes in comparison with the literature-known L^1−L^4-based complexes are given in Table 1 (this includes electronic and Mössbauer

https://doi.org/10.1021/acs.inorgchem.4c01237
Inorg. Chem. 2024, 63, 12109−12119

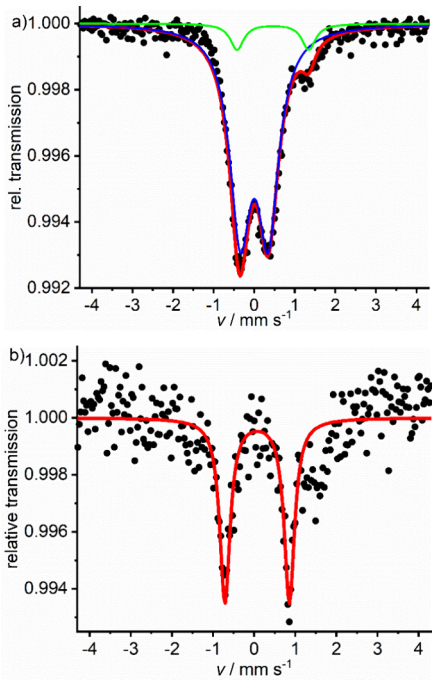

Figure 1. 80 K Mössbauer spectra of frozen solutions of (a) $[(L^5)Fe^{IV}{=}NTs]^{2+}$ (δ = 0.00 mm s^{-1}, $|\Delta E_Q|$ = 0.69 mm s^{-1}, blue subspectrum) containing some unreacted iron(II) precursor (8%, δ = 0.46 mm s^{-1}, $|\Delta E_Q|$ = 1.77 mm s^{-1}, green subspectrum) and (b) $[(L^6)Fe^{IV}{=}NTs]^{2+}$ (δ = 0.07 mm s^{-1}, $|\Delta E_Q|$ = 1.57 mm s^{-1}).

spectroscopic data and, for the latter, also DFT-computed parameters).

For the iron(IV)-oxido complexes, the assignment of the dd transitions is based on a thorough analysis of MCD and UV−vis-NIR spectra of the crystallographically characterized complex with tetramethylcyclam (tmc),[70] and this has also been used to assign the dd transitions in solution spectra of $[(L)Fe^{IV}{=}O(X)]^{n+}$, where L is a tetradentate bispidine derivative with coligands X = NCMe, Cl, Br, on the basis of a thorough ligand field analysis.[42] These assignments are also applicable for $[(L^5)Fe^{IV}{=}O]^{2+}$ and $[(L^6)Fe^{IV}{=}O]^{2+}$: there are generally two main resolved dd transitions in solution spectra, i.e., around 700−800 nm assigned to $d_{xz,yz} \rightarrow d_{x2-y2}$ and at around 500−600 nm assigned to $d_{xz,yz} \rightarrow d_{z2}$ (the latter is not shown in Table 1, since the corresponding transition is not resolved in the solution spectra of $[(L^n)Fe^{IV}{=}NTs]^{2+}$, n = 5, 6). Since the d_{x2-y2} orbital is not influenced by a substitution of the oxido by the tosylimido ligand, one does not expect a significant shift of the lower energy dd transition when comparing the oxido with the corresponding tosylimido species, and this is what emerges from the data in Table 1, specifically for the two bispidine complexes discussed here.

Zero field Mössbauer spectra of $[(L^5)Fe^{IV}{=}NTs]^{2+}$ and $[(L^6)Fe^{IV}{=}NTs]^{2+}$ are shown in Figure 1, and the parameters are listed in Table 1. The isomer shifts and quadrupole splitting are very similar to those of the corresponding oxido complexes and confirm a bonding pattern with Fe^{IV} in a triplet ground state. This is further supported by good agreement of the experimental parameters with the DFT-based computed parameters (Table 1).

The main fragments in the ESI mass spectra of $[(L^5)Fe^{IV}{=}NTs]^{2+}$ and $[(L^6)Fe^{IV}{=}NTs]^{2+}$ appear at m/z = 740.1710, which corresponds to $[(L^n)Fe^{IV}{=}NTs]^{+}$ (n = 5, 6). With the less reactive $[(L^5)Fe^{IV}{=}NTs]^{2+}$, an additional species with very low intensity (m/z = 370.0843), corresponding to the 2+ charged $[(L^5)\ Fe^{IV}{=}NTs]^{2+}$, could also be detected. ESI-tandem-MS shows that the two species with 1+ and 2+ charges are clearly intact tosylimido complexes (see Figure 2). The fact that the 1e$^-$ reduced species is observed as the main species in both systems with the pentadentate bispidines is not unusual for complexes with reactive nitrogen ligands such as tosylamide.[71,72] The presence of any Fe^{IV} oxido impurities can be excluded.

Reactivity of the Bispidine-Iron(IV)-Tosylimido Complexes. Tosylimido group transfer reactions were studied for both bispidine-iron(IV)-tosylimido complexes. Thioanisole is oxidized by PhINTs without a metal-ion-based catalyst and, therefore, could not be used for these experiments. Therefore, aziridination of styrene was employed as a model reaction. The two bispidine-based precatalysts $[(L^5)Fe^{II}(NCMe)]OTf_2$ and $[(L^6)Fe^{II}(NCMe)]OTf_2$ showed catalytic activity with turnover frequencies of 33 h^{-1} (20% yield with respect to the oxidant) and 6 h^{-1} (34% yield), respectively ($[Fe^{II}]$ = 5 mM, 20 eq PhINTs, 100 eq styrene, MeCN, Ar, RT, see Experimental Section for details). These activities were of the same order of efficiency as with the analogous $Cu^{I/II}$ complexes, but, as the iron catalysts are not regarded as competitive, these reactions were not optimized or further studied (see Supporting Information for details of the preliminary data).[24]

The kinetic analyses of the $[(L^n)Fe^{IV}{=}NTs]^{2+}$ oxidants (n = 5, 6) were studied by time-resolved spectra of their characteristic charge transfer or low energy dd transitions ($d_{xz,yz} \rightarrow d_{x2-y2}$, see above). Tosylimido group transfer (NAT) and C−H activation (HAA) were considered. As substrate for the former, we decided to use thioanisole, since the reaction with styrene is significantly slower (hours vs. minutes at RT) and therefore more prone to side reactions. The uncatalyzed background reaction with excess PhINTs also poses no problem if the kinetics of the reactions are determined via

Table 1. Spectroscopic Parameters (UV-vis-NIR, Mössbauer) of the $Fe^{IV}{=}O$ and $Fe^{IV}{=}NTs$ Complexes of L^1−L^6

	L^1 [34]	L^2 [35,38]	L^3 [29,28]	L^4 [29]	L^5 [68]	L^6 [68,69]
UV−vis-NIR	λ_{max} [nm]					
$Fe^{IV}{=}O$	695	739	740	750	730	730
$Fe^{IV}{=}NTs$	660	650	740	750	735	730
Mössbauer	$\delta/\lvert\Delta E_Q\rvert$ [mm·s^{-1}]					
$Fe^{IV}{=}O$, exp	0.04/0.93	0.01/0.87	−0.01/0.93		0.02/0.69	0.01/1.34
$Fe^{IV}{=}O$, calc	0.05/0.93	0.10/0.83	0.09/0.55		0.22/0.17	0.07/1.24
$Fe^{IV}{=}NTs$, exp	0.02/1.03		0.06/0.73	0.05/1.09	0.00/0.69	0.07/1.57
$Fe^{IV}{=}NTs$, calc	0.14/1.33	0.18/1.09	0.04/0.77	0.03/1.01	0.20/0.81	0.17/1.58

https://doi.org/10.1021/acs.inorgchem.4c01237
Inorg. Chem. 2024, 63, 12109−12119

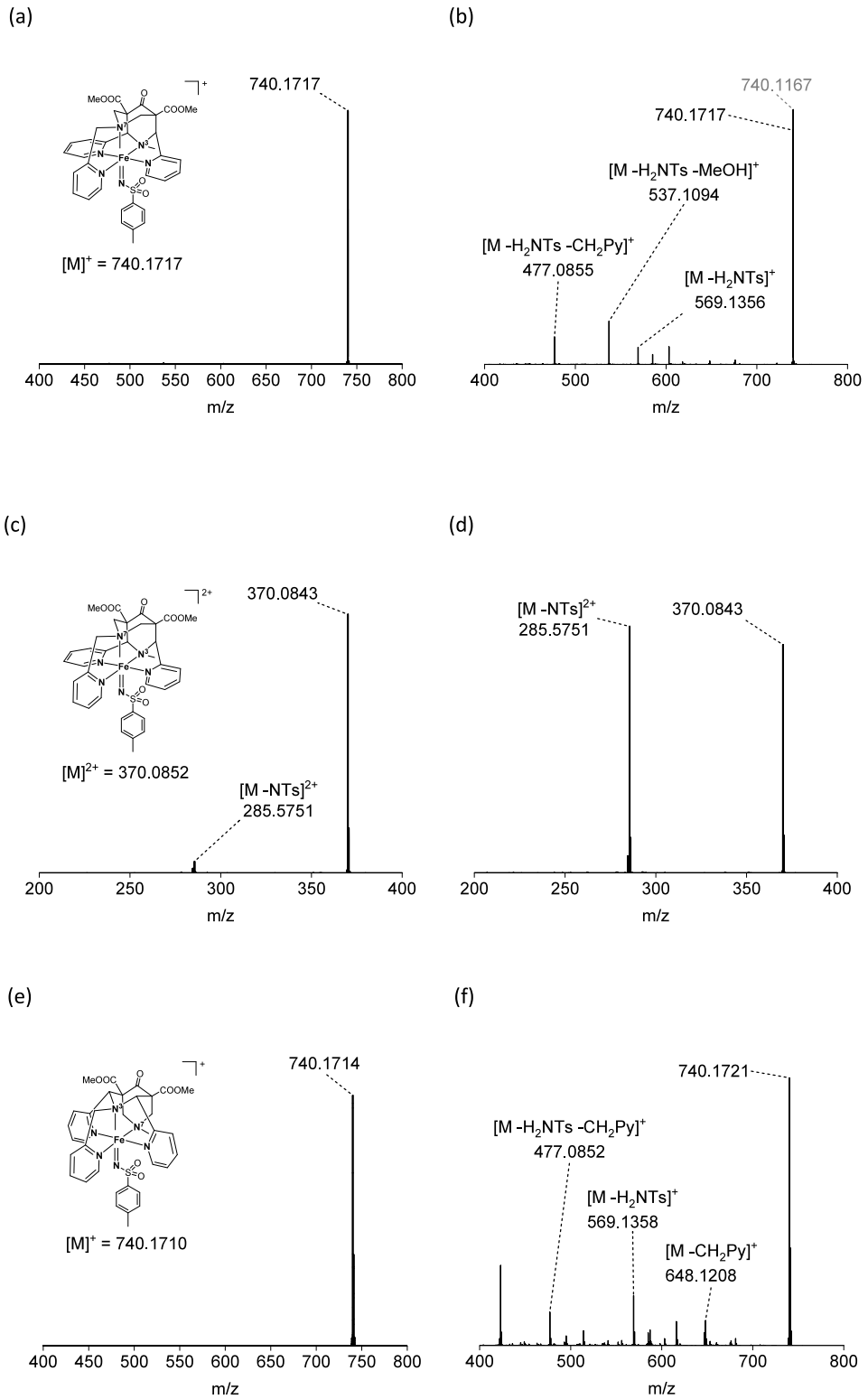

Figure 2. ESI-tandem-MS of iron(IV)-tosylimido complexes. (a) $[(L^6)Fe(NTs)]^+$, i.e., the $1e^-$ reduced species with a calculated m/z = 740.1710, isolated species. (b) fragmentation spectra of m/z = 740.1717 with 20 V acceleration voltage. (c) $[(L^6)Fe(NTs)]^{2+}$ with a calculated m/z = 370.0852, isolated species. (d) fragmentation spectra of m/z = 370.0843 with 10 V acceleration voltage. (e) $[(L^5)Fe(NTs)]^+$, i.e., the $1e^-$ reduced species with a calculated m/z = 740.1710, isolated species. (f) Fragmentation spectra of m/z = 740.1714 with 30 V acceleration voltage.

the characteristic absorption of the high-valent iron oxidant (note that this also ensures that the observed substrate oxidation is due to Fe^{IV} and not any other iron-based oxidant). As substrate for HAA, we have used 1,3-cyclohexadiene (1,3-CHD), since cyclohexane that was used for the corresponding Fe^{IV}═O oxidants[38,40] has a too strong C−H bond (BDE = 99.5 vs 78 kcal/mol),[29,39] leading to very slow reactions, even at ambient temperature.

Reactions of $[(L^5)Fe^{IV}$═$NTs]^{2+}$ and $[(L^6)Fe^{IV}$═$NTs]^{2+}$ (0.5 mM in MeCN, Ar, and RT) with thioanisole (2.5−10

https://doi.org/10.1021/acs.inorgchem.4c01237
Inorg. Chem. 2024, 63, 12109−12119

Table 2. Second-Order Rate Constants (M^{-1} s^{-1}) of the Reactions of $[(L^n)Fe^{IV}{=}O]^{2+}$ and $[(L^n)Fe^{IV}{=}NTs]^{2+}$ with Thioanisole at 298 K, 1,3-Cycohexadiene at 233 K, and for $[(L^n)Fe^{IV}{=}O]^{2+}$ with Cyclohexane at 298 K (where Values in Parentheses Are Given; These Are the Original Data at Deviating Temperatures (See Footnotes)[a]

	$[(L^n)Fe^{IV}{=}O]^{2+}$				$[(L^n)Fe^{IV}{=}NTs]^{2+}$			
	thioanisole		1,3-CHD	cyclohexane	thioanisole		1,3-CHD	
L^1 [37,50,51]	0.49	(0.05 ± 0.004)[b]	0.07 ± 0.003	5.5×10^{-5}	2.6	(0.26 ± 0.003)[b]		
L^2 [34,37,51]	8.2	(0.33)[c]	0.96 ± 0.03	3.9×10^{-4}	0.054			
L^3 [28]	0.14	(0.091 ± 0.004)[d]	0.027 ± 0.001	no reaction	0.012	$(7.9 \times 10^{-3} \pm 8 \times 10^{-4})$[d]		
L^5 [37,44]	5.65 ± 0.10		0.014 ± 0.001	$1.3 \times 10^{-4} \pm 3 \times 10^{-6}$	9.77 ± 0.29		0.0014	(0.554 ± 0.044)[e]
L^6 [37,44]	480 ± 2		0.37 ± 0.02	$4.9 \times 10^{-3} \pm 8 \times 10^{-6}$	117 ± 16		0.012	(4.55 ± 0.57)[e]

[a]In these cases, the data given for the standard temperatures are approximated by van't Hoff's rule, factor of 2.5 per 10 K. [b]T = 273 K. [c]T = 263 K. [d]T = 293 K. [e] [38,67] T = 298 K.

mM) were measured to determine the second-order rate constants k_2 (see Supporting Information for details, Figures S8 and S13). For the HAA kinetics, $[(L^5)Fe^{IV}{=}NTs]^{2+}$ and $[(L^6)Fe^{IV}{=}NTs]^{2+}$ (0.5 mM in MeCN, Ar, RT) were reacted with 1,3-CHD (10−25 mM, $[(L^5)Fe^{IV}{=}NTs]^{2+}$; 20−35 mM, $[(L^6)Fe^{IV}{=}NTs]^{2+}$, see Supporting Information for details, Figures S18 and S23). The second-order rates for the two reactions are tabulated in comparison with the rates of the corresponding oxido complexes and also including data from the other ligand systems, i.e., L^1, L^2, and L^3 (see Table 2). The interpretation of the relative rates given below is based on the assumption that all reactions of the five tosylimido species follow the same pathways, and this is supported by the thorough computational study; see below.

In general, the oxidation rates of the tosylimido species are significantly slower than those of the oxido complexes—there are two exceptions, i.e., the tosylimido group transfer reactions involving the N_4py ligand L^1 and the bispidine L^5, where the reactions with $[(L^n)Fe^{IV}{=}NTs]^{2+}$ are five- or twofold faster than with the analogous $[(L^n)Fe^{IV}{=}O]^{2+}$ complexes. The TS for the tosylimido transfer from $[(L^n)Fe^{IV}{=}NTs]^{2+}$ involves the interaction of the coordinated tosylimido group with the sulfur atom of the thioether, and this occurs, similar to the corresponding oxido transfer from $[(L^n)Fe^{IV}{=}O]^{2+}$ on the quintet surface, while the oxidants generally have a triplet ground state, i.e., spin crossover on the way to the group transfer is required.[35,73] It has been noted that the electron transfer properties of $[(L^n)Fe^{IV}{=}NTs]^{2+}$and $[(L^n)Fe^{IV}{=}O]^{2+}$ as well as the basicities of the corresponding $1e^-$ reduced forms are significantly different,[36,37] and this might be a reason for varying differences in reactivities when comparing analogous oxido and tosylimido complexes. For the HAA reactions, the C−H abstraction is the rate-determining step. For 1,3-CHD, this is followed by a very fast second PCET step, leading to benzene. In the case of cyclohexane, there are three possible follow-up reactions, i.e., rebound to produce cyclohexanol, desaturation (i.e., a second PCET step), and cage escape of the organic radical in the $[(L)Fe^{III}OH]^{2+}$/radical intermediate, and, with significant barriers of these follow-up processes, these might also become kinetically relevant.[43] For both group transfer and HAA reactivity, the driving force of the first and rate-determining step, i.e., the $Fe^{IV/III}$ redox potential, is of importance and, unfortunately only little accurate data is available for this process.[38,74,75] Therefore, interpretation of the trends observed in Table 2 is, to some extent, speculation.

Computational Analysis. The formation of the five iron(IV)-tosylimido complexes with L^n (n = 1, 2, 3, 5, 6) from the corresponding iron(II) precursors has been studied by DFT. The formation free energies for the five complexes in the most stable triplet ground state are in the range of 180−205 kJ/mol, i.e., these complexes are thermodynamically feasible (see Supporting Information for details, Table S1), suggesting facile formation and consistency with earlier reports.[76]

The optimized structures of the iron(IV)-tosylimido complexes $[(L^n)Fe{=}NTs]^{2+}$ (n = 1−3, 5, 6) have an intermediate spin (S = 1) ground state, in agreement with the experimental Mössbauer and electronic spectroscopic data (see above). The good agreement between experimental and computed Mössbauer parameters supports the quality of the optimized structures and the overall charge density at the metal centers. The computed triplet−quintet gaps are 25.7, 12.8, 17.4, 19.5, and 21.3 kJ/mol for the iron(IV)-tosylimido complexes of L^1, L^2, L^3, L^5, and L^6, respectively (see Table S3). The relatively small energy gaps enable the usual two-state reactivity.[77,78] The $Fe^{IV}{=}N$ (NTs) bond lengths in the S = 1 species are 1.745, 1.763, 1.739, 1.759, and 1.768 Å (see Figure 3). There is a relatively large variation (~0.03 Å) in these $Fe^{IV}{=}N$ bond lengths compared to the corresponding $[(L^n)Fe^{IV}{=}O]^{2+}$ complexes (~0.004 Å),[43] but the tertiary amine group *trans* to $Fe^{IV}{=}NTs$ (axial position, see Scheme 1)

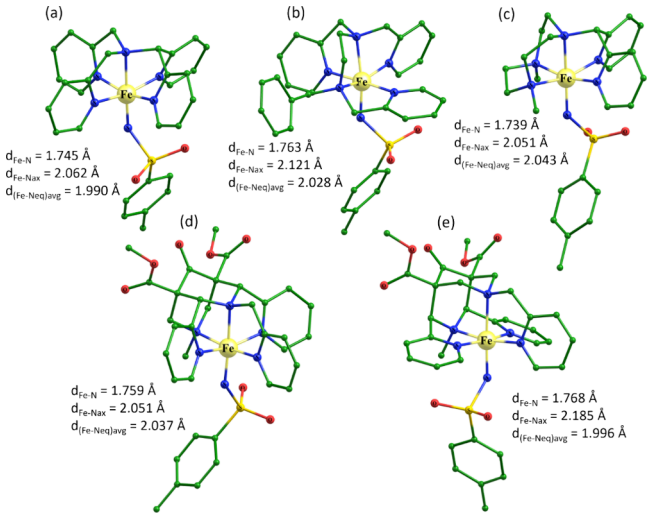

Figure 3. B3LYP-D2-computed ground-state structure of (a) $[(L^1)Fe^{IV}{=}NTs]^{2+}$, (b) $[(L^2)Fe^{IV}{=}NTs]^{2+}$, (c) $[(L^3)Fe^{IV}{=}NTs]^{2+}$, (d) $[(L^5)Fe^{IV}{=}NTs]^{2+}$, and (e) $[(L^6)Fe^{IV}{=}NTs]^{2+}$.

https://doi.org/10.1021/acs.inorgchem.4c01237
Inorg. Chem. 2024, 63, 12109−12119

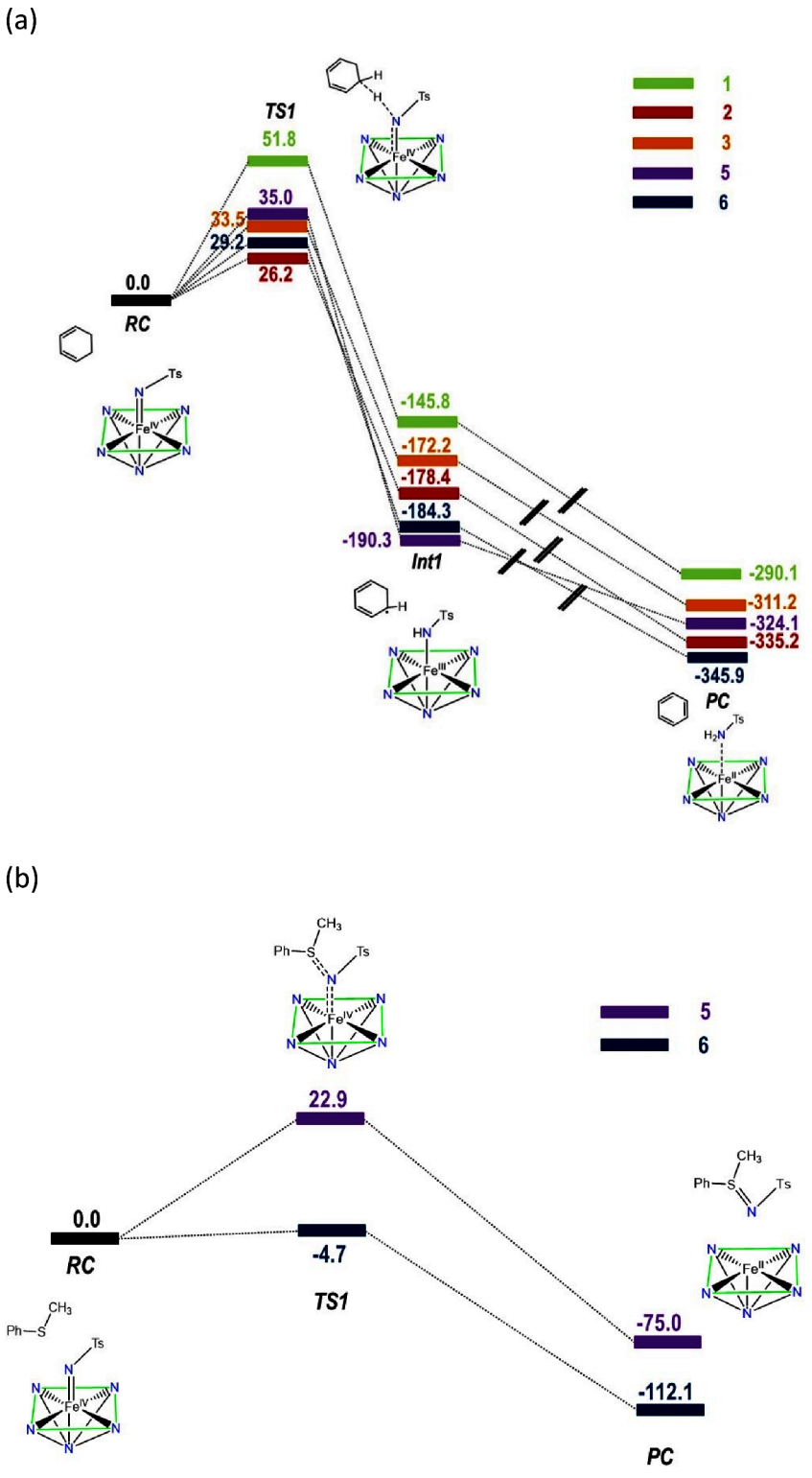

Figure 4. DFT-computed comparative energy profile diagrams (kJ/mol) on the low-lying energy surface of (a) $[(L^n)Fe^{IV}{=}NTs]^{2+}$ complexes (n = 1−3, 5, 6) with 1,3-CHD and (b) $[(L^n)Fe^{IV}{=}NTs]^{2+}$ complexes (n = 5, 6) with thioanisole at the UB3LYP-D2/TZVP(PCM)//UB3LYP-D2/LanL2DZ(Fe),6-31G*(rest atoms) level of theory (see also Supporting Information, Figures S26 and S27).

shows a similar variation as in the $[(L^n)Fe^{IV}{=}O]^{2+}$ complexes [the Fe−N_{ax} (Fe−$N_{eq\ (avg.)}$) distances for the L^1-, L^2-, L^3-, L^5-, and L^6-based complexes are 2.062 (1.990), 2.121 (2.028), 2.051 (2.043), 2.051 (2.037), and 2.185 (1.996) Å, respectively (see Figure 3). Similar to the $[(L^n)Fe^{IV}{=}O]^{2+}$ complexes, the longer Fe−N_{ax} bonds for the L^2- and L^6-based complexes are probably due to ligand enforcement and this may have an influence on the triplet−quintet gap since the high-spin configuration profits from a Jahn−Teller-type stabilization, as well as on the activation barrier.[67]

The reactivity of $[(L^n)Fe^{IV}{=}NTs]^{2+}$ (n = 1−3, 5, 6) was probed by a computational study with 1,3-CHD as a substrate.

https://doi.org/10.1021/acs.inorgchem.4c01237
Inorg. Chem. 2024, 63, 12109−12119

The desaturation of 1,3-CHD is expected to proceed through a C−H bond activation step (via TS1), followed by the formation of a radical intermediate (Int1). The second C−H bond abstraction (via TS2) leads to the formation of benzene as the stable product (P), and this is generally a barrierless process; i.e., TS1 is the only relevant TS (see Figure 4a). In all five complexes, there is a crossover from the triplet in the RC to the quintet in TS1. For example, for $[(L^1)Fe^{IV}{=}NTs]^{2+}$, the DFT-computed barrier to the quintet TS1 is 51.8 kJ/mol while it is 105.5 kJ/mol on the triplet surface (the corresponding energies for all five complexes are 51.8/105.5, 26.2/100.1, 33.5/88.7, 35.0/116.5, and 29.2/94.2 kJ/mol, see Figure 4a and Supporting Information, Table S4). The corresponding barriers with the $[(L^n)Fe^{IV}{=}O]^{2+}$complexes (n = 1−3, 5, 6) on the quintet surfaces are 24.5, 16.8, 35.7, 24.9, and 17.0 kJ/mol,[43] i.e., with the exception of the L^3-based system (with an energy difference that is not significant with the error margins of DFT), the tosylimido oxidants are more sluggish than the oxido complexes, as also observed experimentally for a range of HAA substrates (see Table 2 and Supporting Information, Figures S8, S13, S18, and S23).[29,35,36,53]

To gain more insight into the mechanism of the iron(IV)-tosylimido species, we have also calculated the activation barriers for NAT to thioanisole for the two most reactive complexes $[(L^5)Fe^{IV}{=}NTs]^{2+}$ and $[(L^6)Fe^{IV}{=}NTs]^{2+}$ (for the L^1- and L^2-based complexes, there are published activation barriers that support the general trend although they are at different levels of theory).[36,53] On the lower energy quintet surface, the direct attack of $[(L^5)Fe^{IV}{=}NTs]^{2+}$ and $[(L^6)Fe^{IV}{=}NTs]^{2+}$ to thioanisole has DFT-computed barriers of 22.9 and −4.7 kJ/mol, and the DLPNO-CCSD(T)-computed energy barriers are 40.0 and 10.0 kJ/mol, respectively (see Supporting Information, Table S5). In agreement with computational work involving other ligand systems, the barriers on the triplet surface are significantly higher and the barriers for the L^1- and L^2-based iron(IV)-tosylimido oxidants are higher, in agreement with the experimental data.[36,53] The computed barriers for $[(L^5)Fe^{IV}{=}NTs]^{2+}$ and $[(L^6)Fe^{IV}{=}NTs]^{2+}$ suggest that the two bispidine complexes are the most reactive, with $[(L^6)Fe^{IV}{=}NTs]^{2+}$ significantly more reactive than its isomer, and this is also in agreement with the experimental results (k_2 = 9.77 ± 0.29 M^{-1} s^{-1} ($[(L^5)Fe^{IV}{=}NTs]^{2+}$) and k_2 = 117 ± 16 M^{-1} s^{-1} ($[(L^6)Fe^{IV}{=}NTs]^{2+}$), see Table 2 and Supporting Information, Table S1).

The TSs ^{5}TS1 have very little spin density on the tosylimido N atom, and the change in the spin density on Fe from the RC to the TS is negligible [5: ^{5}RC vs. ^{5}TS1 (4.040 vs 4.034), 6: ^{5}RC vs. ^{5}TS1 (3.996 vs. 4.024), see Figure 5 and Table S8], and this also follows from the only minor variation in the Fe−N (tosylimido) bond length between the ^{5}RC and ^{5}TS1 structures for the two tosylimido bispidine complexes 5 and 6 (see Table S7; note that this also holds for all other $[(L^n)Fe^{IV}{=}NTs]^{2+}$ species, n = 1, 2, 3, 5, 6). It follows that the TSs represent a cation-radical ($PhS^{\bullet+}Me$) attack on these tosylimido-iron complexes, which are partially reduced to Fe^{III}−NTs species by accepting electron density from the substrate during RC formation (see Figure 6). Also shown in Figure 6 is how the mechanism for the oxidation of thioanisole, therefore, differs from that of the iron(IV)-oxido transfer reported previously.

An important observation is that, in general, Fe−N (tosylimido) distances are significantly longer than the Fe−O (oxido) distances in the RCs 5-^{5}RC and 6-^{5}RC and that the Fe−N (tosylimido) distances are nearly constant for the tosylimido species on the way to the TSs 5-^{5}TS1 and 6-^{5}TS1, while they vary significantly for the corresponding oxido complexes. We interpret this as partial electron transfer from the substrate to the RC (see Figure 6c), an effect that has been observed before for $Fe^{IV}{=}NTs$ complexes.[36] An important consequence of this is the significant elongation of the Fe−N vs. Fe−O bond that leads to a reduction of steric strain induced by the approach of the substrate on the way to the TS and, therefore, diminishes the energetic penalty for the corresponding activation barrier. This obviously has a major effect in systems where the ligands are sterically demanding at the atom transfer site. For oxygen atom transfer (OAT), it has been observed that in the series of the $[(L^1)Fe^{IV}{=}O]^{2+}$ to $[(L^6)Fe^{IV}{=}O]^{2+}$ complexes studied here, the reactivities decrease with the number of pyridine groups parallel to the Fe=O bond.[38] The structural drawings of the complexes in Scheme 1 (and the corresponding computed structures throughout) indicate that, therefore, the steric demand of the L^1 (four parallel pyridines) and L^5 (three parallel pyridines)-based complexes will lead to especially high steric strain at the $Fe^{IV}{=}O\cdots$substrate site. For NAT of the tosylimido complexes, the effect of the parallel pyridine rings on the substrate approach is much reduced due to the bond elongation discussed above, and this is a possible explanation for the abovementioned exceptions when one compares the OAT with NAT in the series of the five complexes with L^n (n = 1, 2, 3, 5, 6). Note that, obviously, these steric effects are not the only aspect, i.e., thermodynamics (the redox potential of the high-valent oxidant, *e.g.*, via stabilization of the iron(IV)-oxido species by hydrogen bonds) and electronic effects (spin state, quintet−triplet gap, etc.) are of importance, but the steric effects also play a significant role. In this sense, the L^1- and L^5-based systems are exceptions for the $[(L^n)Fe^{IV}{=}O]^{2+}$ systems, where steric effects are becoming more important than usual, while for the $[(L^n)Fe^{IV}{=}NTs]^{2+}$ systems, steric hindrance is less important due to the longer bonds.

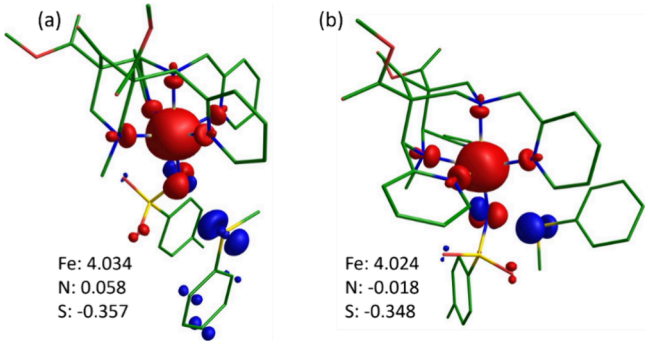

Figure 5. Spin-density plots of the transition states of (a) 5-^{5}TS1 and (b) 6-^{5}TS1 at a contour value of 0.03 au.

CONCLUSIONS

The successful synthesis and thorough spectroscopic characterization of the $[(L^n)Fe^{IV}{=}NTs]^{2+}$ complexes (n = 5, 6) with the two pentadentate isomeric bispidine ligands completes the series of iron(IV)-tosylimido complexes with the pentadentate amine-pyridine ligands L^n (n = 1−3, 5, 6), where the corresponding $[(L^n)Fe^{IV}{=}O]^{2+}$ complexes have been studied in detail, while generally, the $[(L^n)Fe^{IV}{=}NTs]^{2+}$ species are less reactive than the $[(L^n)Fe^{IV}{=}O]^{2+}$ analogues; for the atom

https://doi.org/10.1021/acs.inorgchem.4c01237
Inorg. Chem. 2024, 63, 12109−12119

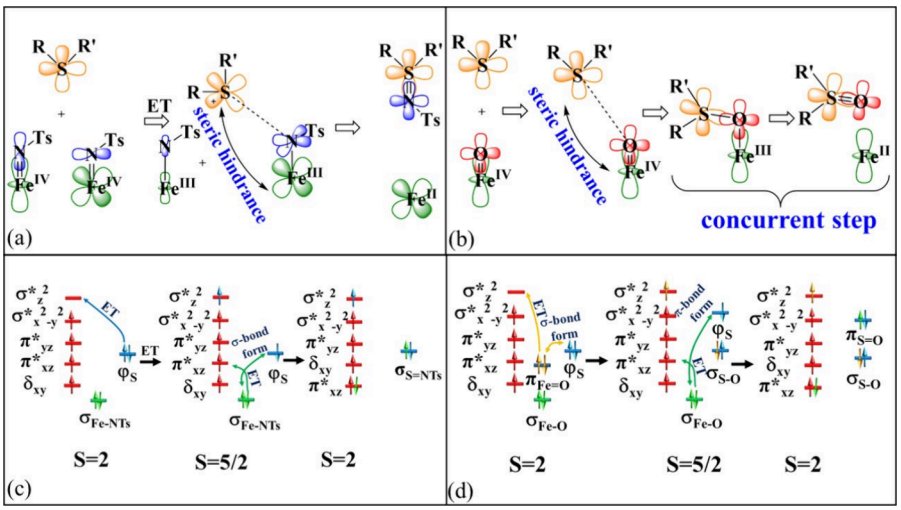

Figure 6. Orbital interaction diagram showing the cleavage and formation of bonds in (a) Fe^{IV}═NTs and (b) Fe^{IV}═O; corresponding electron shift mechanisms (c) for Fe^{IV}═NTs and (d) for Fe^{IV}═O.

transfer reactions to thioanisole, there are two notable exceptions, i.e., those with L^1 and L^5 that show faster NAT than that of OAT by factors of 2 to 5. This is traced back to steric hindrance in the case of the Fe^{IV}═O oxidants, which is reduced in the Fe^{IV}═NT species due to significantly longer Fe^{IV}═N (Fe^{III}–N) bonds than in the case of the Fe^{IV}═O bonds. It is general knowledge that reactivities are a combination of thermodynamics, electronics, and sterics, and it is of importance that this also holds for atom transfer reactions with high-valent nonheme iron oxidants, an aspect that is of notable importance in the series of oxidants studied here.

■ ASSOCIATED CONTENT

Supporting Information

The Supporting Information is available free of charge at https://pubs.acs.org/doi/10.1021/acs.inorgchem.4c01237.

Methods and materials; UV−vis-NIR spectroscopy; kinetics; determination of the aziridination yields; computational work; and coordinates (PDF)

■ AUTHOR INFORMATION

Corresponding Authors

Gopalan Rajaraman − *Department of Chemistry, Indian Institute of Technology Bombay, Mumbai 400076, India;* orcid.org/0000-0001-6133-3026; Email: rajaraman@chem.iitb.ac.in

Peter Comba − *Anorganisch-Chemisches Institut, Universität Heidelberg, Heidelberg D-69120, Germany; Interdisziplinäres Zentrum für Wissenschaftliches Rechnen (IWR), Universität Heidelberg, Heidelberg 69120, Germany;* orcid.org/0000-0001-7796-3532; Email: peter.comba@aci.uni-heidelberg.de

Authors

Thomas Josephy − *Anorganisch-Chemisches Institut, Universität Heidelberg, Heidelberg D-69120, Germany*

Ravi Kumar − *Department of Chemistry, Indian Institute of Technology Bombay, Mumbai 400076, India;* orcid.org/0000-0001-8465-3495

Katharina Bleher − *Anorganisch-Chemisches Institut, Universität Heidelberg, Heidelberg D-69120, Germany;*

Institute of Functional Interfaces, Karlsruhe Institute of Technology, Eggenstein-Leopoldshafen 76344, Germany; orcid.org/0009-0002-0589-9601

Fridolin Röhs − *Lehrstuhl für Anorganische Chemie I, Fakultät für Chemie, Universität Bielefeld, Bielefeld D-33615, Germany*

Thorsten Glaser − *Lehrstuhl für Anorganische Chemie I, Fakultät für Chemie, Universität Bielefeld, Bielefeld D-33615, Germany*

Complete contact information is available at: https://pubs.acs.org/10.1021/acs.inorgchem.4c01237

Author Contributions

#T.J. and R.K. equally contributed to this study.

Notes

The authors declare no competing financial interest.

■ ACKNOWLEDGMENTS

Financial support by the University of Heidelberg is gratefully acknowledged. This study was conducted within the Max Planck School Matter to Life, supported by the BMBF in collaboration with the Max Planck Society. The computational resources were provided by the state of Baden-Württemberg through bwHPC and the German Research Foundation (DFG) through grant no. INST 40/575-1 FUGG (JUSTUS 2 cluster). Financial support by the German Science Foundation (DFG) within the Research Unit FOR 5215 "Bioinspired Oxidation Catalysis with Iron Complexes "BioOxCat") to P.C. (TP4) and T.G. (TP1) is gratefully acknowledged. G.R. would like to thank SERB, India (SB/SJF/2019-20/12; CRG/2022/001697), and the Alexander von Humboldt Foundation for funding.

■ REFERENCES

(1) Krebs, C.; Galonić Fujimori, D.; Walsh, C. T.; Bollinger, J. M. Non-heme Fe (IV)−oxo intermediates. *Acc. Chem. Res.* **2007**, *40*, 484−492.

(2) Abu-Omar, M. M.; Loaiza, A.; Hontzeas, N. Reaction mechanisms of mononuclear non-heme iron oxygenases. *Chem. Rev.* **2005**, *105*, 2227−2252.

(3) Hohenberger, J.; Ray, K.; Meyer, K. The biology and chemistry of high-valent iron−oxo and iron−nitrido complexes. *Nat. Commun.* **2012**, *3*, 720.
(4) Althoff, F.; Benzing, K.; Comba, P.; McRoberts, C.; Boyd, D. R.; Greiner, S.; Keppler, F. Abiotic methanogenesis from organosulphur compounds under ambient conditions. *Nat. Commun.* **2014**, *5* (1), 4205.
(5) Comba, P.; Kerscher, M.; Krause, M.; Schöler, H. F. Iron-catalysed oxidation and halogenation of organic matter in nature. *Env. Chem.* **2015**, *12*, 381−395.
(6) Benzing, K.; Comba, P.; Martin, B.; Pokrandt, B.; Keppler, F. nonheme iron-oxo-catalyzed methane formation from methionine: Scope, mechanism and relevance for natural systems. *Chem. - Eur. J.* **2017**, *23* (43), 10465−10472.
(7) Rana, S.; Biswas, J. P.; Paul, S.; Paik, A.; Maiti, D. Organic synthesis with the most abundant transition metal iron: from rust to multitasking catalysts. *Chem. Soc. Rev.* **2021**, *50*, 243−472.
(8) Vicens, L.; Olivo, G.; Costas, M. Rational design of bioinspired catalysts for selective oxidations. *ACS Catal.* **2020**, *10*, 8611−8631.
(9) Grapperhaus, C. A.; Mienert, B.; Bill, E.; Weyhermüller, T.; Wieghardt, K. Mononuclear (nitrido)iron(V) and (Oxo)iron(IV) Complexes via Photolysis of $[(\text{cyclam-acetato})\text{Fe}^{\text{III}}(\text{N}_3)]^+$ and Ozonolysis of $[(\text{cyclam-acetato})\text{Fe}^{\text{III}}(\text{O}_3\text{SCF}_3)]^+$ in Water/Acetone Mixtures. *Inorg. Chem.* **2000**, *39*, 5306−5317.
(10) Rohde, J.-U.; In, J.-H.; Lim, M. H.; Brennessel, W. W.; Bukowski, M. R.; Stubna, A.; Münck, E.; Nam, W.; Que, L., Jr. Crystallographic and Spectroscopic Characterization of a nonheme Fe^{IV}=O Complex. *Science* **2003**, *299*, 1037−1039.
(11) Price, J. C.; Barr, E. W.; Tirupati, B.; Bollinger, J. M.; Krebs, C. The First Direct Characterization of a High-Valent Iron Intermediate in the Reaction of an α-Ketoglutarate-Dependent Dioxygenase: A High-Spin Fe(IV) Complex in Taurine/α-Ketoglutarate Dioxygenase (TauD) from Escherichia coli. *Biochemistry* **2003**, *42*, 7497−7508.
(12) Nam, W.; Lee, Y.-M.; Fukuzumi, S. Tuning reactivity and mechanism in oxidation reactions by mononuclear nonheme iron (IV)-oxo complexes. *Acc. Chem. Res.* **2014**, *47*, 1146−1154.
(13) Solomon, E. I.; Brunold, T. C.; Davis, M. I.; Kemsley, J. N.; Lee, S. K.; Lehnert, N.; Neese, F.; Skulan, A. J.; Yang, Y. S.; Zhou, J. Geometric and Electronic Structure/Function Correlations in Non-Heme Iron Enzymes. *Chem. Rev.* **2000**, *100*, 235.
(14) Fukuzumi, S.; Cho, K.-B.; Lee, Y.-M.; Hong, S.; Nam, W. Mechanistic dichotomies in redox reactions of mononuclear metal-oxygen intermediates. *Chem. Soc. Rev.* **2020**, *49*, 8988−9027.
(15) Mukherjee, G.; Velmurugan, G.; Kerscher, M.; Kumar Satpathy, J.; Sastri, C. V.; Comba, P. Mechanistic insights into amphoteric reactivity of an iron-bispidine complex. *Chem. - Eur. J.* **2023**, No. e202303127.
(16) Zhu, W.; Wu, P.; Larson, V. A.; Kumar, A.; Li, X.-X.; Seo, M. S.; Lee, Y.-M.; Wang, B.; Lehnert, N.; Nam, W. Electronic structure and reactivity of mononuclear nonheme iro-peroxo complexes as biomimetic model of Rieske oxygenases: ring size effects of macrocyclic ligands. *J. Am. Chem. Soc.* **2024**, *146*, 250−262.
(17) Oloo, W. N.; Que, L., Jr Bioinspired nonheme iron catalysts for C-H and C = C bond oxidation: insights into the nature of the metal-based oxidants. *Acc. Chem. Res.* **2015**, *48*, 2612−2621.
(18) Olivo, G.; Cussó, O.; Borrell, M.; Costas, M. Oxidation of alkane and alkene moieties with biologically inspired nonheme iron catalysts and hydrogen peroxide: from free radicals to stereoselective transformations. *J. Biol. Inorg. Chem.* **2017**, *22*, 425−452.
(19) Jensen, M. P.; Mehn, M. P.; Que, L. Intramolecular Aromatic amination through Iron-Mediated Nitrene Transfer. *Angew. Chem., Int. Ed.* **2003**, *43* (36), 4357−4360.
(20) Avenier, F.; Latour, J.-M. Catalytic aziridination of olefins and amidation of thioanisole by a non-heme iron complex. *Chem. Commun.* **2004**, 1544−1545, DOI: 10.1039/B404561K.
(21) Uchida, T.; Katsuki, T. Asymmetric nitrene transfer reactions: sulfimidation, aziridination and C-H amination using azide compounds as nitrene precursors *Chem. Rec.* **2014**, *14*, 117−129.
(22) Thomas, F.; Oster, M.; Schön, F.; Göbgen, K. C.; Amarouch, B.; Steden, D.; Hoffmann, A.; Herres-Pawlis, S. New Generation of Terminal Copper Nitrenes and Their Application in Aromatic C-H amination Reactions. *Dalton Trans.* **2021**, *50* (19), 6444−6462.
(23) Comba, P.; Haaf, C.; Lienke, A.; Muruganantham, A.; Wadepohl, H. Synthesis, structure and highly efficient copper-catalyzed aziridination with a novel tetraaza-bispidine ligand. *Chem. - Eur. J.* **2009**, *15*, 10880−10887.
(24) Bleher, K.; Comba, P.; Gast, M.; Kronenberger, S.; Josephy, T. Copper-bispidine catalyzed aziridination − a new twist in small molecule activation. *Inorg. Chim. Acta* **2022**, *532* ((SpecialIssue for M. Palanandiavar), No. 120752.
(25) Klotz, K. L.; Slominski, L. M.; Riemer, M. E.; Phillips, J. A.; Halfen, J. A. Mechanism of the iron-mediated alkene aziridination reaction: experimental and computational investigations. *Inorg. Chem.* **2009**, *48*, 801−803.
(26) Klotz, K. L.; Slominski, L. M.; Hull, A. V.; Gottsacker, V. M.; Mas-Ballest, R.; Que, L., Jr.; Halfen, J. A. Non-heme iron(II) complexes are efficient olefin aziridination catalysts. *Chem. Commun.* **2007**, 2063−2065.
(27) Hong, S.; Lu, X.; Lee, Y.-M.; Seo, M. S.; Ohta, T.; Ogura, T.; Clemancey, M.; Maldivi, P.; Latour, J.-M.; Sarangi, R.; et al. Achieving one-electron oxidation of a mononuclear nonheme iron(V)-imido complex. *J. Am. Chem. Soc.* **2017**, *139*, 14372−14375.
(28) Coin, G.; Patra, R.; Rana, S.; Biswas, J. P.; Dubourdeaux, P.; Clémancey, M.; de Visser, S. P.; Maiti, D.; Maldivi, P.; Latour, J. M. Fe-catalyzed aziridination is governed by the electron affinity of the active imido-iron species. *ACS Catal.* **2020**, *10*, 10010−10020.
(29) Sabenya, G.; Gamba, I.; Gómez, L.; Clémancey, M.; Frisch, J. R.; Klinker, E. J.; Blondin, G.; Torelli, S.; Que, L.; Martin-Diaconescu, V.; Latour, J. M.; Lloret-Fillol, J.; Costas, M.; et al. Octahedral iron(IV)-tosylimido complexes exhibiting single electron-oxidation reactivity *Chem. Sci.* **2019**, *10*, 9513−9529.
(30) Verma, A. K.; Nazif, T. N.; Achim, C.; Lee, S. C. A stable terminal imide on iron. *J. Am. Chem. Soc.* **2000**, *122*, 11013−11014.
(31) Brown, S. D.; Betley, T. A.; Peters, J. C. A low-spin d5 iron imide: nitrene capture by low-coordinate iron(I) provides the 4-coordinate Fe(III) complex $[\text{PhB}(\text{CH}_2\text{PPh}_2)_3]\text{Fe}{\equiv}\text{N-p-tolyl}$. *J. Am. Chem. Soc.* **2003**, *125*, 322−323.
(32) Thomas, C. M.; Mankad, N. P.; Peters, J. C. Characterization of the terminal iron(IV) imides $\{[\text{PhBP}^{\text{tBu2}}(\text{pz'})]\text{Fe}^{\text{IV}}{\equiv}\text{NAd}\}^+$. *J. Am. Chem. Soc.* **2006**, *128*, 4956−4957.
(33) Lucas, R. L.; Powell, D. R.; Borovik, A. S. Preparation of iron amido complexes via putative Fe(IV) imido intermediates. *J. Am. Chem. Soc.* **2005**, *127*, 11596−11597.
(34) Klinker, E. J.; Jackson, T. A.; Jensen, M. P.; Stubna, A.; Juhasz, G.; Bominaar, E. L.; Münck, E.; Que, L., Jr. A tosylimido analogue of a nonheme oxoiron(IV) complex. *Angew. Chem., Int. Ed.* **2006**, *45*, 7394−7397.
(35) Mukherjee, G.; Reinhard, F. G. C.; Bagha, U. K.; Sastri, C. V.; de Visser, S. P. Sluggish reactivity by a nonheme iron(IV)-tosylimido complex as compared to its oxo analogue. *Dalton Trans.* **2020**, *49*, 5921−5931.
(36) Kumar, S.; Faponle, A. S.; Barman, P.; Vardhaman, A. K.; Sastri, C. V.; Kumar, D.; de Visser, S. P. Long-range electron transfer triggers mechanistic differences between iron(IV)-oxo and iron(IV)-imido oxidants. *J. Am. Chem. Soc.* **2014**, *136*, 17102−17115.
(37) Vardhaman, A. K.; Lee, Y.-M.; Jung, J.; Ohkubo, K.; Nam, W.; Fukuzumi, S. Enhanced electron transfer reactivity of a nonheme iron(IV)-imido complex as compared to the iron(IV)-oxo analogue. *Angew. Chem., Int. Ed.* **2016**, *55*, 3709−3713.
(38) Wang, D.; Ray, K.; Collins, M. J.; Farquhar, E. R.; Frisch, J. R.; Gomez, L.; Jackson, T. A.; Kerscher, M.; Waleska, A.; Comba, P.; et al. Non-heme oxoiron(IV) complexes of pentadentate N5 ligands: spectroscopy, electrochemistry and oxidative reactivity. *Chem. Sci.* **2013**, *4*, 282−291.
(39) Tian, Z.; Fattahi, A.; Lis, L.; Kass, S. R. Cycloalkane and cycloalkene C-H bond dissociation energies. *J. Am. Chem. Soc.* **2006**, *128*, 17087.

(40) Abu-Odeh, M.; Bleher, K.; Johnee Britto, N.; Comba, P.; Gast, M.; Jaccob, M.; Kerscher, M.; Krieg, S.; Kurth, M. Pathways of the extremely reactive iron(IV)oxido complexes with tetradentate bispidine ligands. *Chem. - Eur. J.* **2021**, *27*, 11377−11390.
(41) Bleher, K.; Comba, P.; Faltermeier, D.; Gupta, A.; Kerscher, M.; Krieg, S.; Martin, B.; Velmurugan, G.; Yang, S. Non-heme-iron-catalyzed halogenation of unactivated carbon-hydrogen bonds. *Chem. - Eur. J.* **2022**, *27*, No. e202103452.
(42) Comba, P.; Nunn, G.; Scherz, F.; Walton, P. H. Intermediate-spin iron(IV)-oxido species with record reactivity. *Faraday Discuss.* **2022**, *234*, 232−244.
(43) Kumar, R.; Ansari, A.; Comba, P.; Rajaraman, G. Rebound or cage escape? The role of the rebound barrier for the reactivity o non-heme high-valent Fe^{IV}=O species. *Chem. - Eur. J.* **2023**, No. e202303300.
(44) Evans, D. A.; Faul, M. M.; Bilodeau, M. T. Development of the copper-catalyzed olefin aziridination reaction. *J. Am. Chem. Soc.* **1994**, *116*, 2742−2753.
(45) Evans, D. A.; Faul, M. M.; Bilodeau, M. T. Copper-catalyzed aziridination of olefins by (N-(p-toluenesulfonyl)imino)-phenyliodinane. *J. Org. Chem.* **1991**, *56*, 6744−6746.
(46) Yamada, Y.; Yamamoto, T.; Okawara, M. Synthesis and reaction of new type I-N ylide, n-tosyliminoiodinane. *Chemistry Letters* **1975**, *4*, 361−362.
(47) Mannich, C.; Mohs, P. Über Derivate eines aus zwei Piperidinringen kondensierten bicyclischen Systems. *Chem. Ber.* **1930**, *B63*, 608−612.
(48) Börzel, H.; Comba, P.; Hagen, K. S.; Merz, M.; Lampeka, Y. D.; Lienke, A.; Linti, G.; Pritzkow, H.; Tsymbal, L. V. Iron coordination chemistry with tetra-, penta- and hexadentate bispidine-type ligands. *Inorg. Chim. Acta* **2002**, *337*, 407−419.
(49) Comba, P.; Kerscher, M.; Schiek, W. bispidine coordination chemistry. *Prog. Inorg. Chem.* **2007**, *55*, 613−704.
(50) Kumar, R.; Pandey, B.; Rajaraman, G. Comparative oxidative ability of iron (III)-iodosylarene vs. high-valent iron (IV/V)-oxo species: Is lower oxidation state a key to enhance selectivity in organic transformations? *J. Indian Chem. Soc.* **2019**, *96*, 825−836.
(51) Kumar, R.; Ansari, A.; Rajaraman, G. Axial vs. equatorial ligand rivalry in controlling the reactivity of iron(IV)-oxo species: single-state vs. two-state reactivity. *Chem. - Eur. J.* **2018**, *24*, 6818−6827.
(52) Kumar, R.; Sundararajan, M.; Rajaraman, G. A six-coordinate high-spin FeIV = O species of cucurbit[5]uril: a highly potent catalyst for C−H hydroxylation of methane, if synthesised. *Chem. Commun.* **2021**, *57* (100), 13760−13763.
(53) Vardhaman, A. K.; Barman, P.; Kumar, S.; Sastri, C. V.; Kumar, D.; de Visser, S. P. Comparison of the reactivity of nonheme iron(IV)-oxo versus iron(IV)-imido complexes: which is the better oxidant *Angew. Chem. Int. Ed.* **2013**, *52*, 12288−12292.
(54) Frisch, M. J.; Trucks, G. W.; Schlegel, H. B.; Scuseria, G. E.; Robb, M. A.; Cheeseman, J. R.; Scalmani, G.; Barone, V.; Mennucci, B.; Petersson, G. A.et al.; *Gaussian 09, Revision D.01*; Gaussian 09, Revision D.01; Gaussian, Inc.: Wallingford CT, 2009.
(55) Neese, F. ″Software update: the ORCA program system, version 4.0.″. *Wiley Interdisciplinary Reviews: Computational Molecular. Science* **2018**, *8* (1), No. e1327.
(56) Neese, F. The ORCA program system. *Wiley Interdiscip. Rev. Comput. Mol. Sci.* **2012**, *2* (1), 73−78.
(57) Grimme, S. Semiempirical GGA-type density functional constructed with a long-range dispersion correction. *J. Comput. Chem.* **2006**, *27* (15), 1787−1799.
(58) Hay, P. J.; Wadt, W. R. Ab-initio effective core potentials for molecular calculations - potentials for the transition-metal atoms Sc to Hg. *J. Chem. Phys.* **1985**, *82*, 270−283.
(59) Wadt, W. R.; Hay, P. J. Ab-initio effective core potentials for molecular calculations - potentials for main group elements Na to Bi. *J. Chem. Phys.* **1985**, *82*, 284−298.
(60) Hay, P. J.; Wadt, W. R. *J. Chem. Phys.* **1985**, *82*, 299−310.
(61) Ditchfield, R.; Hehre, W. J.; Pople, J. A. *J. Chem. Phys.* **1971**, *54*, 724−728.
(62) Mennucci, B. Polarizable continuum model. *Wiley Interdiscip. Rev. Comput. Mol. Sci.* **2012**, *2* (3), 386−404.
(63) Römelt, M.; Ye, S.; Neese, F. Calibration of modern density functional theory methods for the prediction of ^{57}Fe Mössbauer isomer shifts: meta-GGA and double-hybrid functionals. *Inorg. Chem.* **2009**, *48* (3), 784−785.
(64) Comba, P.; Faltermeier, D.; Krieg, S.; Martin, B.; Rajaraman, G. Spin state of iron(IV)oxido complexes with tetradentate bispidin ligands. *Dalton Trans.* **2020**, *49*, 2888−2894.
(65) Neale, S. E.; Pantazis, D. A.; Macgregor, S. A. Accurate computed spin-state energetics for Co(III) complexes: implications for modelling homogeneous catalysis. *Dalton Trans.* **2020**, *49* (19), 6478−6487.
(66) Comba, P.; Maurer, M.; Vadivelu, P. Oxidation of cyclohexane by a high-valent iron bispidine complex − a combined experimental and computational mechanistic study. *J. Phys. Chem. (A)* **2008**, *112*, 13028−13036.
(67) Comba, P.; Fukuzumi, S.; Koke, C.; Martin, B.; Löhr, A.; Straub, J. A bispidine iron(IV) oxo complex in the entatic state. *Angew. Chem., Int. Ed.* **2016**, *55*, 11129−11133.
(68) Bautz, J.; Bukowski, M.; Kerscher, M.; Stubna, A.; Comba, P.; Lienke, A.; Münck, E.; Que, L., Jr Aqueous oxoiron(IV) formation at pH 2−6 from a nonheme Iron(II) complex and H_2O_2. *Angew. Chem., Int. Ed.* **2006**, *45*, 5681.
(69) Krieg, S. Heidelberg University: Heidelberg, 2019.
(70) Decker, A.; Rohde, J. U.; Que, L.; Solomon, E. I. Spectroscopic and quantum chemical characterization of the electronic structure and bonding in a non-heme Fe(IV)═O complex. *J. Am. Chem. Soc.* **2004**, *126*, 5378−5379.
(71) Gross, J. H.Principles of Ionization and Ion Dissociation. In *Mass Spectronemy*, 3rd ed.; Springer, 2017; pp 29−84.
(72) Bleher, K.; Comba, P.; Gross, J.; Josephy, T. ESI and tandem MS for mechanistic studies of high-valent metal complexes. *Dalton Trans. (Perspective)* **2022**, *51*, 8625−8639.
(73) Jaccob, M.; Comba, P.; Maurer, M.; Vadivelu, P.; Venuvanalingam, P. A combined experimental and computational study on the sulfoxidation by high-valent iron bispidine complexes. *Dalton Trans.* **2011**, *40*, 11276−11281.
(74) Comba, P.; Wadepohl, H.; Waleska, A. Redox properties of iron complexes with pentadentate bispidine ligands. *Aust. J. Chem.* **2014**, *67*, 398−404. *(Heron 6 Special Issue)*
(75) Comba, P.; Löhr, A.-M.; Pfaff, F.; Ray, K. Redox potentials of high-valent iron-, cobalt-, and nickel-oxido complexes: evidence for exchange enhanced reactivity. *Isr. J. Chem.* **2020**, *60*, 957−962. *(Metal-oxido Special Issue)*
(76) Jaccob, M.; Rajaraman, G. A computational examination on the structure, spin state energetics and spectroscopic parameters of high-valent Fe^{IV}=NTs species. *Dalton Trans.* **2012**, *41*, 10430−10439.
(77) Schröder, D.; Shaik, S.; Schwarz, H. Two-state reactivity as a new concept in organometallic chemistry. *Acc. Chem. Res.* **2000**, *33*, 139−145.
(78) Usharani, D.; Janardanan, D.; Li, C.; Shaik, S. A theory for bioinorganic chemical reactivity of oxometal complexes and analogous oxidants: the exchange and orbital−selection rules. *Acc. Chem. Res.* **2013**, *46*, 471−482.

https://doi.org/10.1021/acs.inorgchem.4c01237
Inorg. Chem. 2024, 63, 12109−12119